Korean J. Chem. Eng., 34(10), 2764-2772 (2017)
DOI: 10.1007/s11814-017-0169-z

pISSN: 0256-1115
eISSN: 1975-7220

High textured carbon from chemical vapor infiltration with ethanol precursor and its rate of pyrolytic carbon deposition

Si Won Choi, Kyung Do Joo, and Gui-Yung Chung†

Department of Chemical Engineering, Hongik University, 94 Wausanro, Mapogu, Seoul 04066, Korea
(*Received 13 March 2017 • accepted 20 June 2017*)

Abstract−Preparation of C/C composites with ethanol precursor was studied and the role of ethanol in obtaining high textured (HT) carbon was confirmed. HT carbon was obtained more with ethanol precursor than with propane precursor as reported by Ren et al. The pyrolytic carbon deposition rate constant from ethanol precursor, which has never been reported before in any other research, was obtained. It was confirmed that a proper mixture precursor of ethanol and propane could be used in the process of temperature gradient chemical vapor infiltration (TG-CVI) on behalf of the uniform deposition throughout the preform and the deposition with more HT carbon,. The pyrolytic carbon deposition rate constant for the CVI with propane precursor obtained in this research was 2.2-times greater than that reported by Vaidyaraman.

Keywords: High Textured (HT) Carbon, Ethanol, Propane, C/C Composites, TG-CVI

INTRODUCTION

An archetypal composite is the carbon/carbon composite [1-3] and the chemical vapor infiltration (CVI) is a prominent method of producing this composite. There are numerous types of CVI, such as isothermal-CVI, pulse-CVI, and temperature gradient (TG)-CVI [4-7]. Since deposition rates depend on temperature in the preform, non-uniform depositions might occur due to a non-uniformity of temperature. This non-uniformity can be compensated by the concentration gradient in the preform [8,9]. This method is called TG-CVI and it has been used in this research. The numerical simulations for the various CVI processes have been also studied by many researchers [10-13]. The mathematical modellings were accustomed to optimizing parameters of the CVI processes [14-19]. In this research pyrolytic carbon deposition rate constants were obtained by fitting modelling results to experimental data.

Ren et al. [20-22] grouped the pyrolytic carbons into four classes: high texture (HT), medium texture (MT), low texture (LT), and isotropic. They identified classes of carbons with the polarized light microscopy (PLM) images. The PLM images of fibers in the preform are black as they are not sensitive to light, while the deposited HT pyrolytic carbon has a high optical activity and exhibits irregular and rough extinction crosses [23]. HT carbon was reported to have excellent wear resistance and friction properties than the other deposited carbons [20,24].

In previous researches the hydroxyl group in ethanol has been known to oxidize pyrolytic carbon in the process of vapor deposition. But, in recent papers reported by Ren et al. [20,21], the advantages of oxygen contained in the ethanol have been noticed. They obtained more HT carbon with the ethanol precursor. Furthermore, they used the mixture precursor of ethanol and methane in order to enhance the efficiency of the C/C composite production. HT pyrolytic carbon can be yielded in a small temperature and pressure range with the methane-only precursor. They mentioned that the only role of methane was in increasing diffusivity. So the addition of methane into the pure ethanol precursor improved the densification rate of C/C composites. They concluded that the HT carbon could be obtained effectively using the mixture precursor rather than the pure methane, and ethanol played a critical role in formation of the HT pyrolytic carbon. They reported that the HT carbon was obtained with an optimum ratio of both species [21]. Similarly, the mixture gas of ethanol and propane was used as the precursor gas in this research. Propane was included instead of methane, since more carbons can be deposited from one mole of propane precursor.

The rate constant of pyrolytic carbon deposition from ethanol precursor has not been reported in the previous researches yet. So we tried to induce it from the gas phase reaction rate in this research. Li et al. reported that many reactions occur in the gas phase reactions when ethanol decomposes in the reactor [25]. The following reaction among them is the main gas phase reaction path in the initial stages of the decomposition.

$$C_2H_5OH \rightarrow CH_3^+ + CH_2OH^-;\ k_{EtOH} = 2.59\times10^{54}\ T^{-11.99} e^{(-50576/T)} \quad (1)$$

Here, T [K] is the reaction temperature. The methyl radicals produced in Eq. (1) can be considered as starting materials to deposit pyrolytic carbons. Then, the pyrolytic carbon deposition rate constant from ethanol, i.e., $k_{s\text{-}EtOH}$, can be the multiplication of the adjusting factor (α_{adj}) and the gas phase reaction rate constant (k_{EtOH}) in Eq. (1). This adjusting factor (α_{adj}) could be decided in the process of fitting modeling results to experimental data of the amount of deposition in this research.

On the other hand, the surface deposition reaction of pyrolytic carbon from propane precursor has been reported by Vaidyaraman

†To whom correspondence should be addressed.
E-mail: gychung@hongik.ac.kr

et al. [24] and it was used in this research. They assumed that the surface deposition of carbon is a first-order reaction with respect to the concentration of propane as follows:

$$C_3H_8 \rightarrow 3C_{(s)} + 4H_2 \quad (2)$$

They reported the rate constant of carbon deposition from propane, $k_{s\text{-}Prop}$ [cm/s], as follows:

$$k_{s\text{-}Prop\ by\ Vaidyaraman} = 9.025e^{-\frac{23610}{RT}} \quad (3)$$

Here, R [cal/gmol·K] is the gas constant and T [K] the reaction temperature. The activation energy is 23.6 kcal/mol which is less than 48-60 kcal/mol reported in the reference [26].

In this research, C/C composites were prepared by the CVI with three different precursors: (i) ethanol precursor, (ii) propane precursor, and (iii) mixture precursor of ethanol and propane. For three different precursors, appearance of HT carbon was observed with PLM and SEM photographs. In addition, the amounts of deposition in several parts of each preform were measured and compared with the modeling results. In these processes the overall rate constants of pyrolytic carbon deposition were decided.

EXPERIMENTAL

The experimental system of CVI for the preparation of C/C composites consists of the infiltration reactor and the gas inlet- and outlet-parts as shown in Fig. 1. Ethanol and propane were used as the precursor gases. Ethanol precursor was introduced by bubbling argon gas. Annular preform was used and its shape and dimensions are shown in Fig. 2 and Table 1. Thermocouples were positioned in the central hole and at the outside of the preform. So a temperature gradient along the r-direction in the preform, i.e., 820 °C at the inside rim and 900 °C at the outside surface, could be set during the infiltration processes.

The infiltration process is as follows. A preform was dehydrated in an oven, weighed, and mounted in the sample holder. The reactor was heated under the atmosphere of inert gas, argon. The infiltration was carried out by injecting the precursor and the carrier gas after setting a desired temperature distribution in the preform.

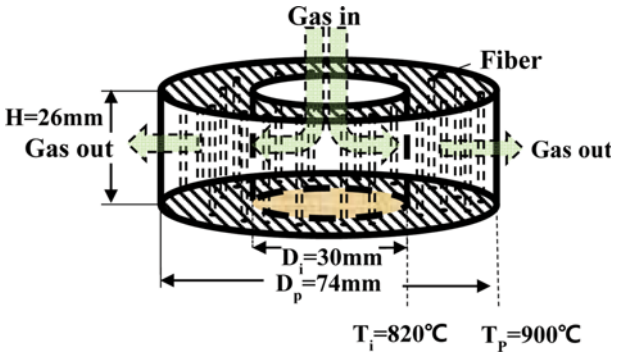

Fig. 2. Schematic diagram of the annular preform. The precursor gas flew down through the central hole and passed out radially from inside to outside through the porous preform.

Table 1. Dimensions of the preform and the infiltration conditions

Dimensions of preform	Inside radius	1.5 cm
	Outside radius	3.7 cm
	Height	2.6 cm
	Initial porosity	0.8418
	Initial density	0.41 g/cm^3
	Number of fibers per unit cross-sectional area	4.11×10^5/cm^2
	Initial radius of fiber	3.5 μm
Operating conditions	Absolute pressure	30 torr
	Flow rate	30 sccm
	Temperature	840-900 °C

After the infiltration reaction, the reactor was cooled under the inert gas atmosphere and the preform was taken out. Then, the bulk density and the amount of deposition in the whole preform were measured. After the preform was cut into five pieces along the r-direction, the amounts of deposition and the densities in those pieces were also measured.

PLM photographs were taken with PLM (Nikon ECLIPSE E600 POL). Photographs of deposited carbon on the lateral surfaces of fibers in the infiltrated preform were taken with SEM (Nanoeyes SNE 1500M).

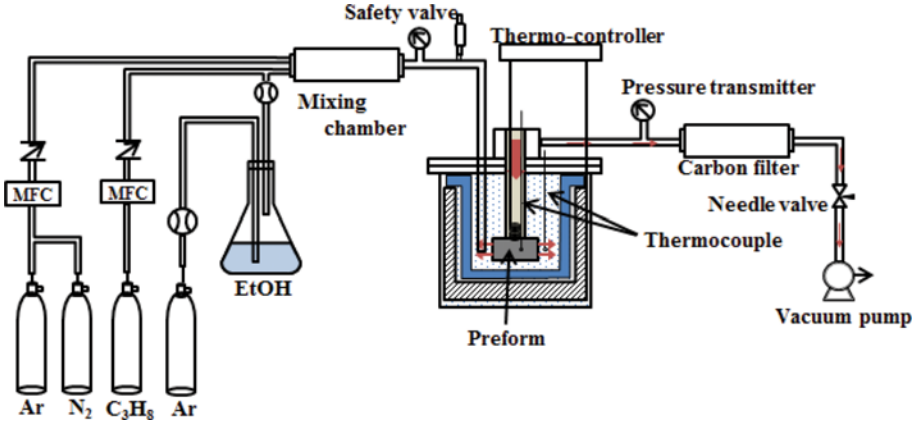

Fig. 1. Schematic diagram of the CVI system.

MODEL DEVELOPMENT

A schematic diagram of the preform used in the mathematical modeling is shown in Fig. 2. The annular preform consisted of fibers. It was assumed that pores were distributed evenly among fibers throughout the whole preform. Precursor gas flowed down through the central hole and went out radially from the center to the outside of the annular preform as shown in Fig. 2.

The mass balance equations for the precursor gas such as ethanol or propane in the system are as follows. A pseudo-steady state was assumed for the concentration distribution in the pores of the preform. There are r- and z-directional diffusions and r-directional convection in the pores among fibers in the preform. The radius of fiber (r_f [cm]), the number of fibers per unit cross-sectional area of the preform (N_f [#/cm^{-2}]) and the mole number of carbons deposited from one mole of precursor gas (q_C) were included, since the surface deposition rate depends on the surface area in addition to the gas phase reaction rate.

$$\frac{1}{r}\frac{\partial}{\partial r}(rJ_r)-\frac{\partial}{\partial z}(J_z)+\frac{1}{r}\frac{\partial}{\partial r}(rv_rC)-\frac{1}{q_C}k_sC2\pi r_fN_f=0 \tag{4}$$

$$\text{b.c. at } z=0 \text{ \& H, } R_i\le r\le R_P;\ \frac{\partial C}{\partial z}=0 \tag{5}$$

$$\text{at } r=R_i \text{ \& all z; } C=C_0 \tag{6}$$

$$\text{at } r=R_P \text{ \& all z; } \frac{\partial C}{\partial r}=0 \tag{7}$$

Here, r and z [cm] are the radial- and the axial-directional coordinates in the preform and J_r and J_z [mol·cm^{-2}·s^{-1}] the r- and z-directional diffusion fluxes of precursor gas, respectively. v_r [cm·s^{-1}] is the gas velocity in the r-direction, k_s [cm·s^{-1}] the first-order surface carbon deposition rate constant, C [mol·cm^{-3}] the concentration of precursor gas. H is the height of the preform. R_i and R_P [cm] are the inside radius and the outside radius of annular preform, respectively. The fourth term is the depletion of precursor gas due to surface deposition on the outside lateral surfaces of fibers in the preform.

The time change of fiber radius at (r, z) in the preform is obtained as follows.

$$\frac{\partial r_{f,r,z}}{\partial t}=\frac{q_CMw_C}{\rho_m}k_sC \tag{8}$$

$$\text{i.c. at } t=0 \text{ all r \& z; } r_{f,r,z}=r_{f0} \tag{9}$$

Here, $r_{f,r,z}$ [cm] is the local radius of fiber, t [s] deposition time, q_C the mole number of deposited carbons per one mole of precursor gas, i.e., 2 for ethanol precursor and 3 for propane precursor, Mw_C the molecular weight of carbon, ρ_m [g/cm^3] the density of deposited carbon, and C [mol/cm^3] the concentration of precursor gas, ethanol or propane. For the mixture precursor of ethanol and propane, the time changes of fiber radius due to depositions of carbons were calculated as the sum of changes due to both precursors.

As mentioned, the pyrolytic carbon deposition rate constant from ethanol precursor, ($k_{s\text{-}EtOH}$), has not been reported yet. So it could be decided based upon the gas phase reaction rate constant (k_{EtOH} in Eq. (1)) in the process of fitting the experimental data to the modeling results of the amount of deposition in this research. Firstly, an adjusting factor (α_{adj}) was obtained in the fitting process.

$$k_{s\text{-}EtOH}=\alpha_{adj}k_{EtOH}=\alpha_{dep}\left(\frac{\varepsilon}{2\pi N_f r_f}\right)_{avg}k_{EtOH} \tag{10}$$

The equation in the parenthesis is a conversion factor from gas phase rate constant (k [s^{-1}]) to surface deposition rate constant (k_s [cm·s^{-1}]). Here the deposition factor (α_{dep}) is the molar number of pyrolytic carbon deposits per one mole of methyl radical generated.

On the other hand, the pyrolytic carbon deposition rate constant from propane precursor, ($k_{s\text{-}Prop}$), was reported by Vaidyaraman et al. [24] as Eq. (3) and it was adjusted and used in this research.

The amount of deposition (D) and the local porosity ($\varepsilon_{r,z}$) in the preform are as follows.

$$D=\rho_m\pi\sum_{z=0}^{H}\sum_{r=R_i}^{R_P}(r_{f,r,z}^2-r_{f0}^2)(N_f2\pi r\Delta r)\Delta z \tag{11}$$

$$\varepsilon_{r,z}=1-\pi r_{f,r,z}^2N_f \tag{12}$$

Here, r_{f0} [cm] is the initial radius of fiber.

All equations were changed into dimensionless forms with the dimensionless parameters such as $\sigma(=r_f/r_{f0})$, $\zeta(=(r-R_i)/(R_P-R_i))$, $\xi(=z/H)$ and calculated by the finite difference method.

RESULTS AND DISCUSSION

To see the effects of ethanol precursor on the properties of deposits and the rate of deposition, CVI's with precursors of (i) ethanol, (ii) propane, and (iii) mixture of both gases were carried out. The types of deposited carbons for three different precursors were compared with the PLM images of deposits after infiltrations. Numerical modellings of these infiltration processes were also made and compared with the experimental data. In these processes, the pyrolytic carbon deposition rate constants for each precursor were decided.

1. PLM Photographs

PLM photographs of the preforms (a) before CVI, (b) after CVI with the ethanol-only precursor, (c) after CVI with the propane-only precursor, and (d) after CVI with the mixture precursor of propane and ethanol are shown in Fig. 3. Nothing was identified in the PLM photograph of fibers before deposition in Fig. 3(a), since fibers in the preform were not sensitive to light. The PLM photographs of fibers after deposition with the ethanol precursor in Fig. 3(b) and with the mixture precursor of propane and ethanol in Fig. 3(d) had many white shapes due to the reflections from the HT carbons. However, the PLM photograph of fibers after deposition with the propane-only precursor in Fig. 3(c) did not have so much white shapes. So it could be confirmed that the HT carbon could be deposited considerably with the precursor including ethanol as reported by Ren et al. [20,21].

2. Rate of Pyrolytic Carbon Deposition

2-1. CVI with Ethanol Precursor

Time changes of the average amount of pyrolytic carbon deposit per unit volume in the whole preform for the ethanol precursor

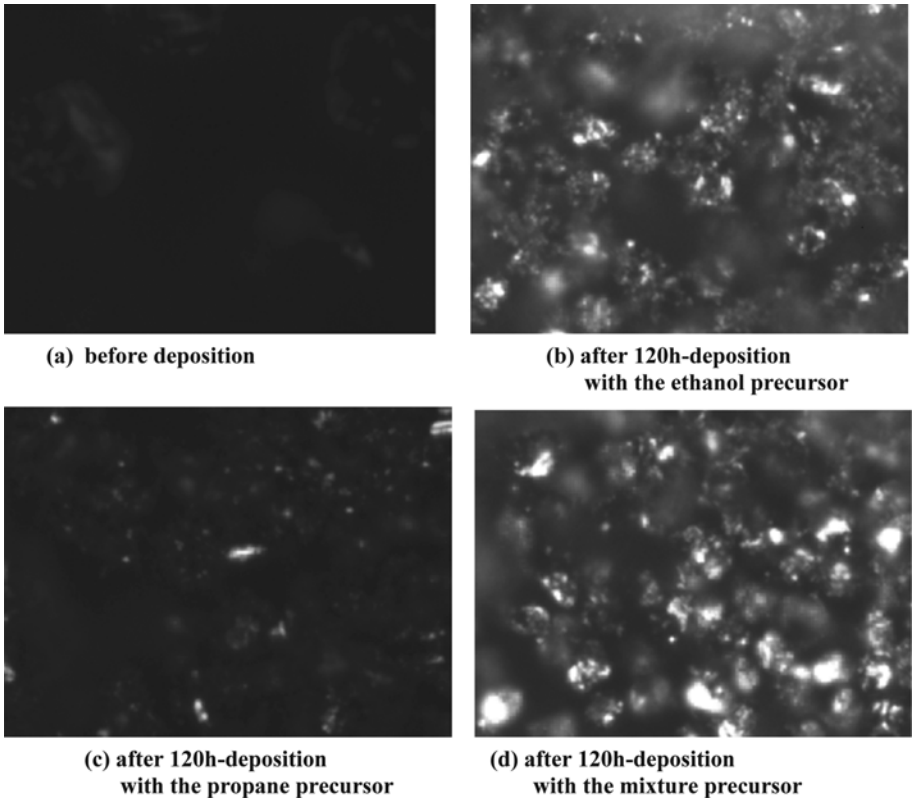

Fig. 3. PLM photographs of the preform (a) before deposition, (b) after deposition with the ethanol-only precursor, (c) after deposition with the propane-only precursor, and (d) after deposition with the mixture precursor of ethanol and propane. Deposition conditions were 120 h, 900 °C, 10% propane, and 10% ethanol. Magnifications of photographs were 800.

are in Fig. 4. Dots are experimental data. The average amount of deposit per unit volume increased almost linearly with time in spite of the decreasing porosity. That is because the rate of pyrolytic carbon deposition depends on the concentration, diffusivity, and the surface area. So the increases of the lateral surface area around cylindrical fibers due to the increasing radii of carbon fibers could have covered the decrease of porosity.

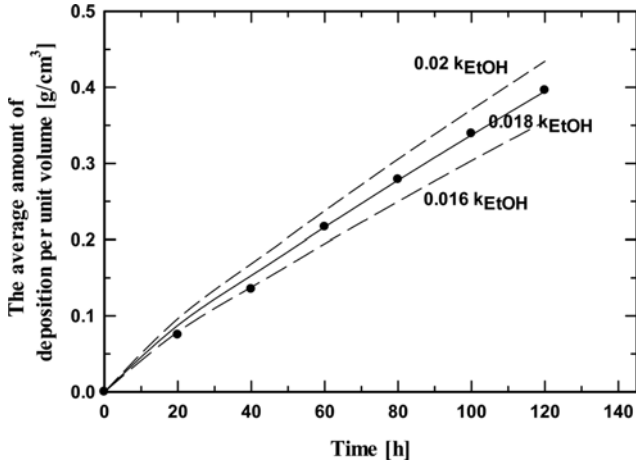

Fig. 4. Time changes of the amount of surface carbon deposition per unit volume in the whole preform in case of ethanol precursor. Deposition conditions were 10% ethanol, 30 torr, and 100 sccm. Dots are experimental data and curves are the results of numerical modelling. Here, k_{EtOH} is the gas phase reaction rate constant of ethanol in Eq. (1) reported by Li et al. [23].

As mentioned in the introduction, the rate constant of pyrolytic carbon deposition from ethanol precursor has not been reported yet. So, the gas phase decomposition rate of ethanol, i.e., k_{EtOH} in Eq. (1), was used with an adjusting factor (α_{adj}) for the numerical modeling in this research. When $0.018k_{EtOH}$ was used as the sur-

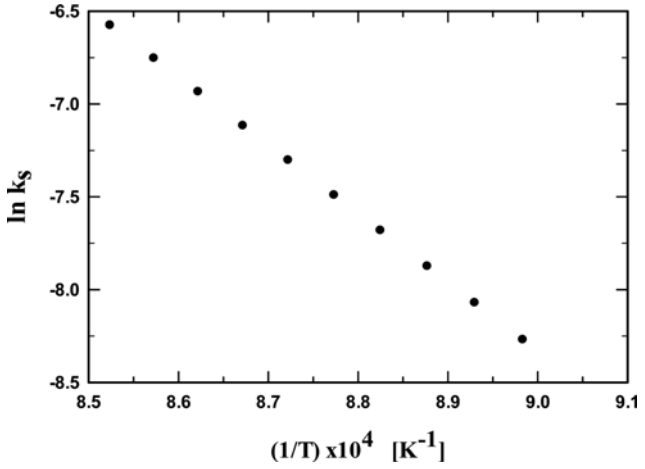

Fig. 5. Arrhenius plot for the pyrolytic carbon deposition reaction for the ethanol precursor.

face deposition rate constant ($k_{s\text{-}EtOH}$), the modeling results of the amount of deposition vs. time fitted the experimental data well as in Fig. 4. Thus, the value of α_{adj} was 0.018. Then the deposition factor (α_{dep}) in Eq. (10) became 19.3. Here, the deposition factor (α_{dep}) is the molar number of pyrolytic carbon deposits through all the reaction paths in the system when one mole of methyl radical is generated.

The rate constant ($k_{s\text{-}EtOH}$) for the pyrolytic carbon deposition from ethanol precursor was drawn into the Arrhenius plot, $\ln(k_{s\text{-}EtOH})$ vs. 1/T, in Fig. 5. The slope and the intercept of the line were −36876 and 24.86, respectively. Hence, the following Eq. (13) was used as $k_{s\text{-}EtOH}$ in the rest of the modeling calculations.

$$\ln(k_{s\text{-}EtOH}) = 24.86 - \frac{36876}{T} = 24.86 - \frac{73273}{RT} \quad (13)$$

R is the gas constant, 1.987 [cal·mol^{-1}K^{-1}]. Hence, for the rate constant of the pyrolytic carbon deposition from ethanol precursor, the pre-exponential factor is 6.26×10^{10} and the activation energy is 73.27 kcal/mol, which is larger than that for the propane precursor reported by Vaidyaraman et al. [24].

2-2. CVI with Propane Precursor

Changes of the average amount of carbon deposition in the whole preform from propane precursor with time are in Fig. 6. Dots are experimental data. As seen for the ethanol precursor, the amount of deposition per unit volume increases with time in spite of the decreasing porosity, as expected. Vaidyaraman et al. [24] reported $k_{s\text{-}Prop}$, the overall pyrolytic carbon deposition rate constant for the propane precursor as in Eq. (3). Modeling results (curves) of the time changes of the amount of deposition per unit volume fitted the experimental data (dots) quite well after multiplying an adjusted parameter of 2.2 to the value of $k_{s\text{-}Prop}$ as shown in Fig. 6. This means that more depositions appeared than predicted with the value of $k_{s\text{-}Prop}$ reported by Vaidyaraman [24], even though the reasons of the discrepancy could not be explained clearly.

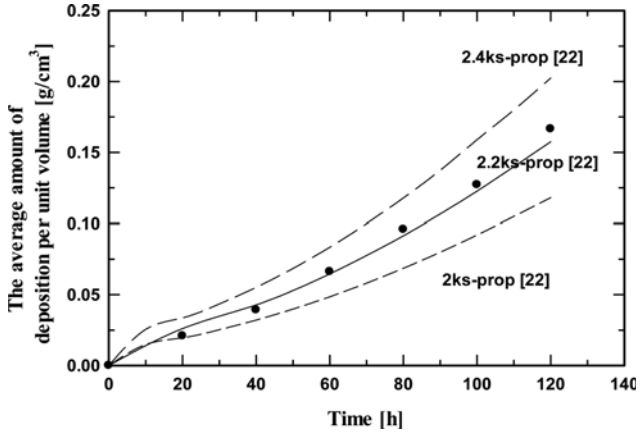

Fig. 6. Time changes of the average amount of pyrolytic carbon deposition per unit volume in the whole preform for the propane precursor. Deposition conditions were 10% propane, 30 torr, and 100 sccm. Dots are experimental data and curves are the results of numerical modelling. Here, $k_{s\text{-}Prop}$ [22] is the overall pyrolytic carbon deposition rate constant for the propane precursor reported by Vaidyaraman et al. [22].

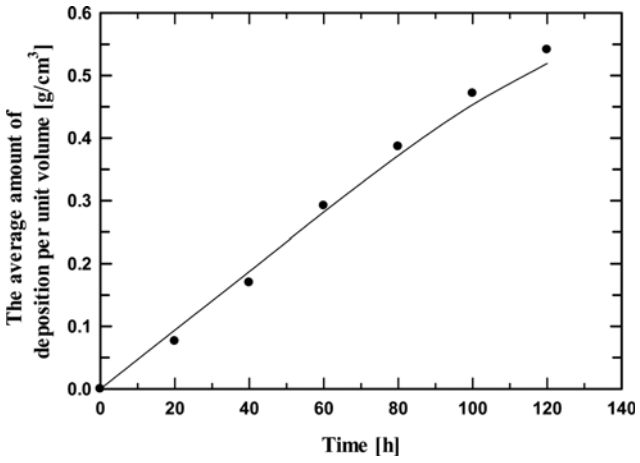

Fig. 7. Time changes of the average amount of pyrolytic carbon deposition per unit volume in the whole preform for the mixture precursor of ethanol and propane. Deposition conditions were 10% ethanol, 10% propane, 30 torr, and 100 sccm. Dots are experimental data and the curve is the result of numerical modelling.

Hence, the following Eq. (14), i.e., $2.2k_{s\text{-}Prop\ by\ Vaidyaranan}$, was used in the rest of the modeling calculations.

$$k_{s\text{-}Prop} = 19.855e^{-\frac{23610}{RT}} \quad (14)$$

2-3. CVI with Mixture Precursor of Ethanol and Propane

Time changes of average pyrolytic carbon deposition per unit volume are in Fig. 7. Modeling results (curve) fit the experimental data (dots) very well. This can be one proof that the estimated pyrolytic carbon deposition rate constants of $k_{s\text{-}EtOH}$ in Eq. (13) for the ethanol precursor and $k_{s\text{-}Prop}$ in Eq. (14) for the propane precursor are reasonable.

The pyrolytic carbon deposition rate constants for ethanol precursor and propane precursor calculated at temperatures along the r-direction in the preform in this research are shown in Fig. 8. The sizes of these two deposition rate constants are similar near the

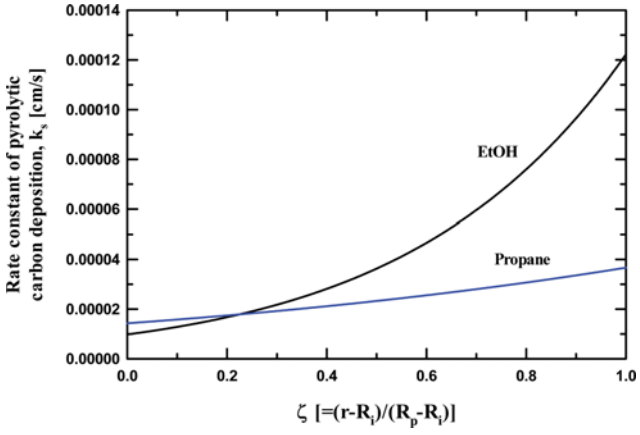

Fig. 8. The rate constants of pyrolytic carbon deposition along the r-direction in the preform for ethanol and propane precursors in this research.

inner radius (Ri). But that for ethanol precursor increases very fast along the r-direction compared with that for propane precursor. This means that the deposition rate constant for ethanol precursor is more sensitive to temperature. So the deposition rate constant for ethanol precursor is much larger at the outer side of the cylindrical preform. As a result, the average amount of deposition per unit volume in the whole preform for ethanol precursor in Fig. 4 was greater than that for propane precursor in Fig. 6.

3. Radial Distributions of Pyrolytic Carbon Deposits throughout the Preform

3-1. CVI with Ethanol Precursor

To fill pores in the preform fully with deposits, the deposits should distribute evenly at all positions in the preform. Hence, to check if deposits were distributed evenly throughout the preform after the CVI process, the amounts of deposits per unit volume along the r-direction at several positions of the preform were measured in the middle of the deposition process and are shown in Fig. 9. Dots are experimental data. Curves are modeling results calculated with $k_{s\text{-}EtOH}$ in Eq. (13) and they fit the experimental data relatively well.

In Fig. 9, deposits were distributed relatively evenly along the r-direction in the preform initially at 20 h. However, the non-uniformity along the r-direction of the deposit-distribution increased as the process time went on. Thus, the amount of deposits near the central hole of the annular preform became considerably more than that near the outer side of the preform. This can be explained as follows. The concentration of ethanol precursor was high and temperature was low near the central hole during the deposition process. However, the deposition rate constant of ethanol at low temperatures but with a high concentration near the central hole was high enough to consume most of precursor gas. So the amount of deposits per unit volume decreased along the r-direction. In addition, the effect of fast consumption of precursor gas due to a high concentration in spite of a low temperature appeared greater as the deposition time went on. So the non-uniformity of deposition along the r-direction increased as the deposition time went on.

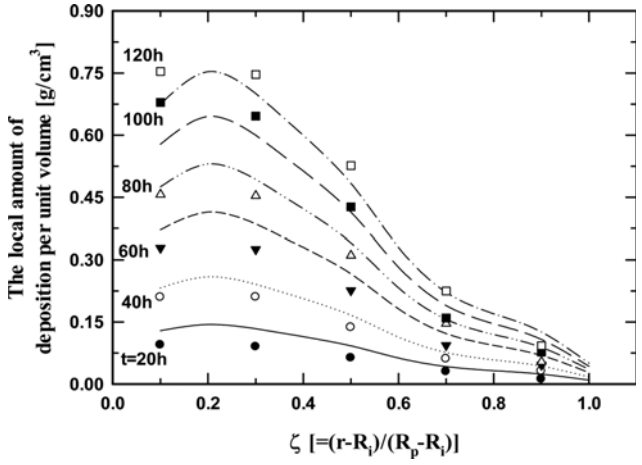

Fig. 9. Radial distributions of the amount of deposited carbon per unit volume in the preform at different deposition times for the ethanol precursor. Dots are experimental data and curves are modeling results calculated with $k_{s\text{-}EtOH}$ in Eq. (13). Deposition conditions were 10% ethanol, 30 torr, and 100 sccm.

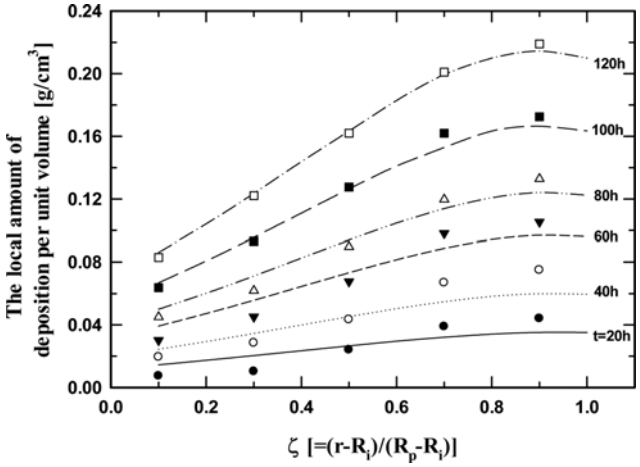

Fig. 10. Radial distributions of the amount of deposited carbon per unit volume in the preform at different deposition times for the propane precursor. Dots are experimental data and curves are modeling results calculated with $k_{s\text{-}Prop}$ in Eq. (14). Deposition conditions were 10% propane, 30 torr, and 100 sccm.

3-2. CVI with Propane Precursor

The measured amounts of deposits per unit volume at several points along the r-direction in the preform at different times are in Fig. 10. Modeling results calculated with the adjusted rate constant, in Eq. (14) fit the experimental data relatively well.

It is desirable to keep temperature low where the concentration is high to get a uniform deposition. Distributions of temperature and concentrations in our experimental system were set in this way as shown in Fig. 1. In our system, the precursor gas flowed along the r-direction from the central hole to the outside of the preform. So the concentration of propane was high and the temperature was low near the central hole ($r=R_i$). On the other hand, those were vice versa near the outside radius ($r=R_p$).

The radial distribution of the amount of deposits per unit volume from CVI with the propane precursor in Fig. 10 is increasing along the r-direction. They are quite different from those with the ethanol precursor in Fig. 9. This is because the rate of deposition near the central hole is not fast enough to consume all of propane gas because of the low temperature in spite of the high concentration. So the amount of deposits could increase along the r-direction because of the increasing temperature.

3-3. CVI with Mixture Precursor of Ethanol and Propane

Radial-distributions of the amount of carbon deposits per unit volume in the preform at different process times are given in Fig. 11. Again, the modeling results calculated with $k_{s\text{-}EtOH}$ in Eq. (13) for ethanol and $k_{s\text{-}Prop}$ in Eq. (14) for propane fitted the experimental data comparatively well.

Radial distributions of the amount of deposits per unit volume for the mixture precursor in Fig. 11 increased like those for the propane precursor. But they are quite unlike those for the ethanol precursor. This means that the trend of the radial distribution of the amount of deposits from CVI with the mixture precursor looks like that from CVI with propane precursor, even though the appearance of HT carbon from CVI with mixture precursor looks

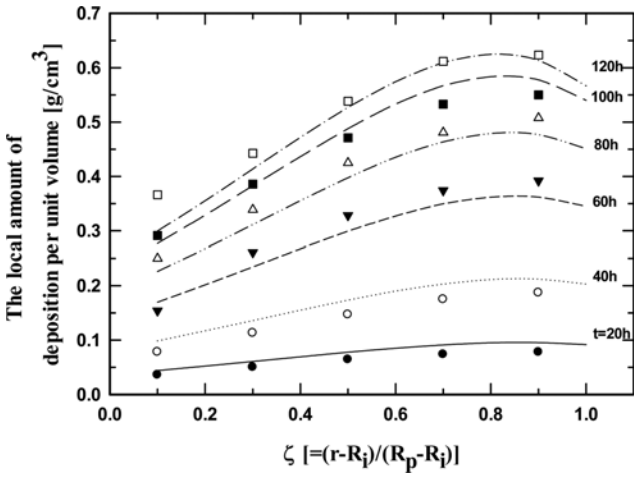

Fig. 11. Radial-distributions of the amount of deposited carbon per unit volume in the preform at different deposition times for the mixture precursor. Dots are experimental data and curves are modeling results calculated with $k_{s\text{-}EtOH}$ in Eq. (13) and $k_{s\text{-}Prop}$ in Eq. (14). Deposition conditions were 10% ethanol, 10% propane, 30 torr, and 100 sccm.

like that from CVI with ethanol precursor as shown in Fig. 3(d).

The amount of pyrolytic carbon deposit was distributed more uniformly along the r-direction than those for ethanol precursor in Fig. 9 and those for propane precursor in Fig. 10. This is one advantage of using a mixture precursor. Again, the non-uniformity of deposition along the r-direction in Fig. 11 increased as time went on.

When the radial- distributions of deposited carbon per unit volume in the preform after 20h-CVI with the ethanol precursor in Fig. 9, the propane precursor in Fig. 10, and the mixture precursor in Fig. 11 are compared, the trends of curves are quite different. The deposited carbon per unit volume decreased along the r-direction for ethanol precursor. However, it increased along the r-direction for propane precursor and mixture precursor. Again, this is because the pyrolytic carbon deposition rate constant for ethanol precursor at 820 °C was high enough to deposit much carbon. So ethanol precursor had been depleted right away after it entered into the preform through the central hole as shown in Fig. 12(a). So little ethane remained at the outer part of the preform. Therefore there were very little deposits even if temperature was high (900 °C) at the outer part of the preform.

On the other hand, for propane precursor, propane remained to react at the outer part of the preform as shown in Fig. 12(b). In addition, the temperature was high at the outer part of the preform. So the deposited carbon per unit volume increased along the r-direction for propane precursor and mixture precursor.

4. SEM Photographs

As depositions on the lateral surfaces of cylindrical fibers in the preform went on, radius of fibers became larger and sizes of pores among fibers became smaller. SEM photographs of the cross-sections of preforms before CVI and after 120 h-CVI are shown in Fig. 13. The shells of cylindrical fibers after CVI in Fig. 13(b), (c), and (d) are deposited pyrolytic carbon. When SEM photographs of preforms after CVI (b) with ethanol precursor and (c) with propane precursor were compared, more deposits were seen in the

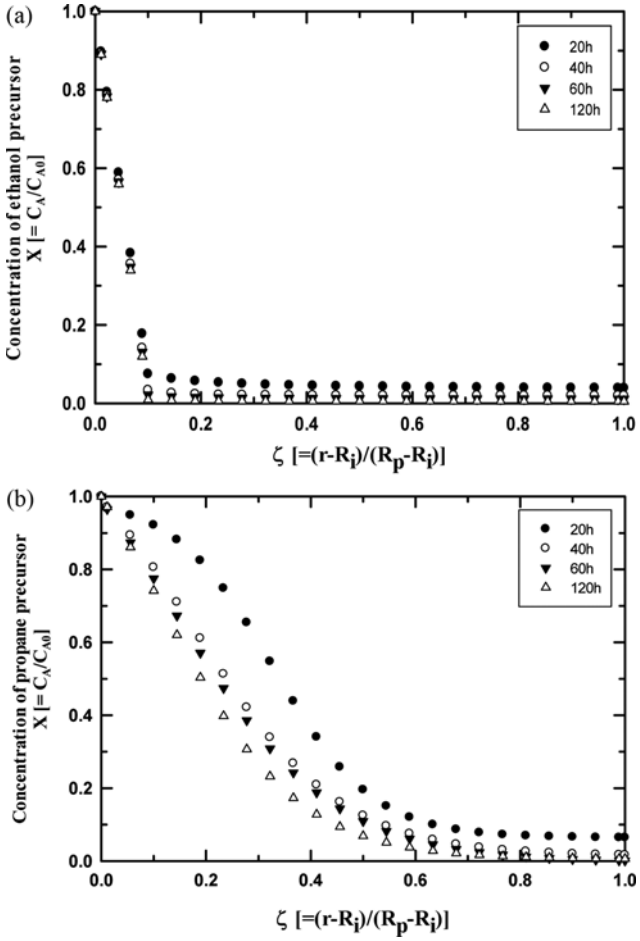

Fig. 12. Radial-distributions of the local concentrations in the preform at 20, 40, 60, and 120 h. (a) for the ethanol precursor and (b) for the propane precursor. Curves were calculated with $k_{s\text{-}EtOH}$ in Eq. (13) and $k_{s\text{-}Prop}$ in Eq. (14). The concentrations of precursors entering through the central hole (C_{A0}) were 10%.

preform after CVI with ethanol precursor. Especially, more deposits were clearly seen in the SEM photograph (d) of the preform after CVI with the mixture precursor. It could be concluded that the ethanol precursor resulted in more deposits than did the propane precursor. Furthermore, the differences between preforms after CVI with ethanol, propane, and mixture precursors could be also felt and identified easily by touch and vision of the preforms. Preforms deposited with the mixture precursor were stiffer and had more deposited pyrolytic carbon.

The end of the deposition process, when pores on the outside surfaces of the preform are plugged with deposits, is 1,100 h in Fig. 14. So 120 h in Fig. 14, the end of the experimental data, can be an early stage of the whole CVI process of 1,100 h. Therefore, pores could be still left vacant even after 120 h-deposition as shown in SEM photographs of Fig. 13(b) and (c).

CONCLUSIONS

Experimental and modeling studies on the preparation of C/C

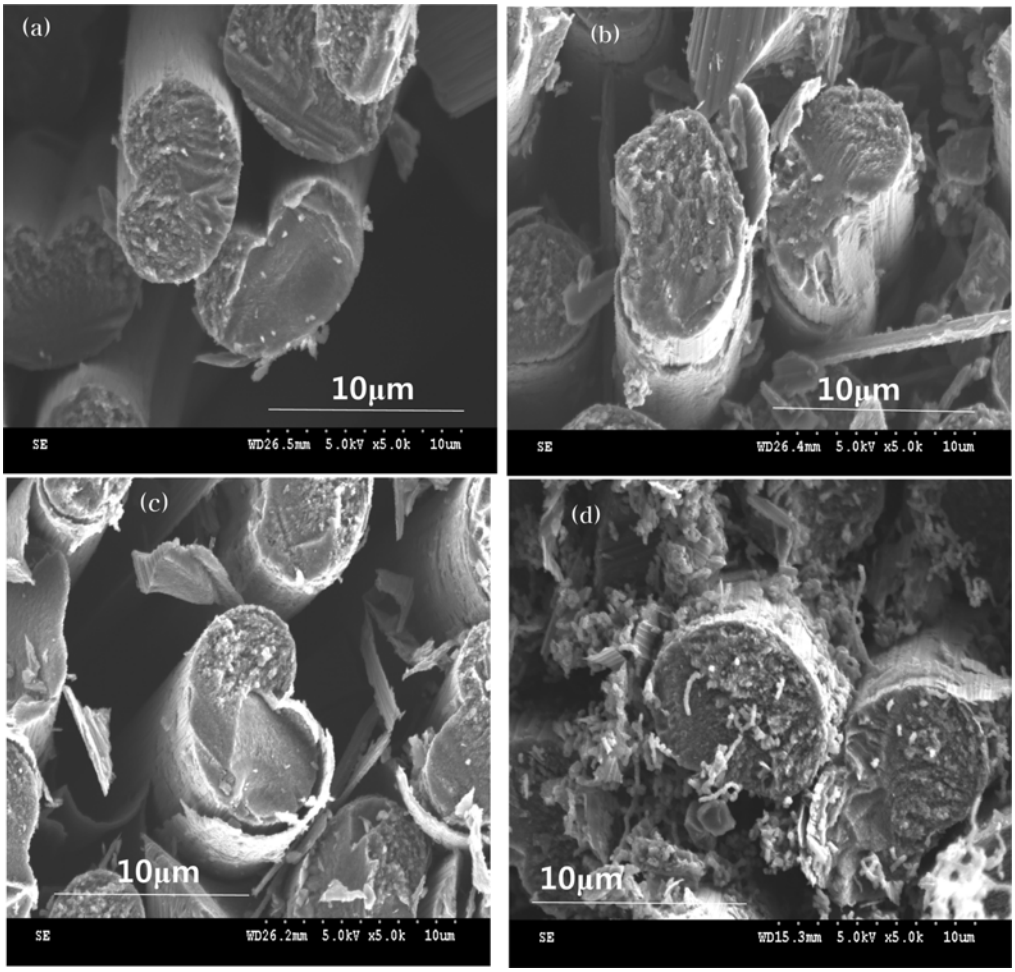

Fig. 13. SEM photographs of the cross-sections of the preforms (a) before CVI, (b) after CVI with ethanol precursor, (c) after CVI with propane precursor, and (d) after CVI with mixture precursor of ethanol and propane. Conditions of CVI: 100 sccm, 10% precursor, 30 torr, 120 h deposition time.

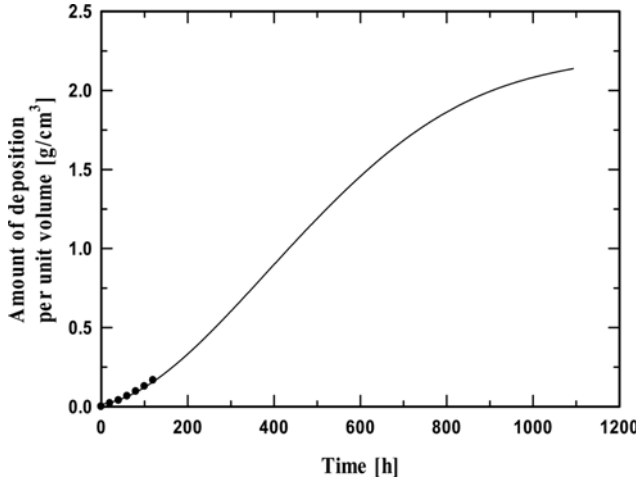

Fig. 14. Time Changes of the average amount of carbon deposition per unit volume in the whole preform during CVI with the propane precursor up to the surface-pore plugging time. It was calculated with $k_{s\text{-}Prop}$ in Eq. (14). Deposition conditions were 10% propane, 30 torr, and 100 sccm. Dots are experimental data.

composites by the TG-CVI were carried out using ethanol precursor, propane precursor, and the mixture precursor of propane and ethanol. The appearance of HT pyrolytic carbon from the CVI with ethanol precursor was observed with PLM photos. In addition, the role of propane in the mixture precursor was also observed. The amounts of deposition in all portions of the annulus carbon fiber preform were calculated by the mathematical modeling, and compared with experimental data. The following conclusions were obtained.

1. The HT carbon could be deposited considerably with a precursor including ethanol as reported by Ren et al. [20,21].

2. Propane in the mixture precursor increased the amount of deposits and contributed in obtaining uniformly distributed deposits in the preform.

3. The rate constant for the pyrolytic carbon deposition from ethanol precursor ($k_{s\text{-}EtOH}$) was exp(24.86-73,273/RT). The activation energy was 73.27 kcal/mol.

4. The rate constant for the pyrolytic carbon deposition from propane precursor ($k_{s\text{-}Prop}$) was 2.2-times bigger than that reported by by Vaidyaraman [24].

5. When a mixture precursor of propane and ethanol was used,

the amounts of deposition in each part of the preform were more uniform in our system because of the different temperature dependencies of the deposition rate constants of propane and ethanol.

6. This research showed that a more uniform deposition throughout the preform can be obtained with a mixture precursor gas and a proper temperature gradient in the preform.

7. Preforms deposited with the precursor including ethanol were stiffer and had more HT pyrolytic carbon. The differences could be identified with SEM photographs.

ACKNOWLEDGEMENTS

This work was supported by the Basic Science Research Program through the National Research Foundation of Korea (NRF) funded by the Ministry of Science, ICT and Future Planning (NRF-2013R1A1A2007280). This research was also supported by the 2016 Hongik University Research Fund.

NOMENCLATURE

C : concentration of precursor [mol/cm^3]
D : amount of deposition [g/cm^3]
J : diffusion flux [mol/cm^2·s]
k_s : rate constant of the pyrolytic carbon deposition [cm/s]
k_{EtOH} : rate constant of the gas phase decomposition of ethanol [/s]
Mw : molecular weight [g/gmol]
N_f : number of fibers per unit cross-sectional area of the preform [/cm^2]
q : number of moles of pyrolytic carbon deposited from one mole of precursor
R : gas constant [cal/gmol·K]
R_i : inside radius of the annular preform [cm]
R_p : outside radius of the annular preform [cm]
r : radius of the preform [cm]
r_f : radius of fiber [cm]
T : temperature [K]
t : deposition time [s]
v : gas velocity [cm/s]

Greek Letters

α : correction factor
ε : porosity
ρ_m : density of pyrolytic carbon [g/cm^3]
ζ : dimensionless parameter of radius

Subscripts

C : deposited pyrolytic carbon
EtOH : ethanol precursor
0 : initial value
Prop : propane precursor
r : radial-directional coordinate in the preform
s : surface
z : axial-directional coordinate in the preform

REFERENCES

1. X. Yang, Z. Su, Q. Huang, X. Fang and L. Chai, *J. Mater. Sci. Technol.*, **29**, 702 (2013).
2. T. Chen, B. Reznik, D. Gerthsen, W. Zhang and K. Hüttinger, *Carbon*, **43**, 3088 (2005).
3. H. C. Shao, H. Y. Xia, G. W. Liu, G. J. Qiao, Z. C. Xiao, J. M. Su, X. H. Zhang and Y. J. Li, *J. Mater. Eng. Perform.*, **23**, 133 (2014).
4. H. J. Li, X. H. Hou and Y. X. Chen, *Carbon*, **38**, 423 (2000).
5. P. Dupel, R. Pailler and F. Langlais, *J. Mater. Sci.*, **29**, 1341 (1994).
6. S. Vaidyaraman, W. J. Lackey, G. B. Freeman, P. K. Agrawal and M. D. Langman, *J. Mater. Res.*, **10**, 1469 (1995).
7. B. J. Kim, D. Han, S. Yoo and S. G. Im, *Korean J. Chem. Eng.*, **34**, 892 (2017).
8. D. K. Rollins Sr., D. J. Rollins and A. D. Jones Jr., *Chem. Eng. Res. Design*, **85**, 1390 (2007).
9. S. Vaidyaraman, W. J. Lackey, P. K. Agrawal, G. B. Freeman and M. A. Miller, *Carbon*, **34**, 347 (1996).
10. G. Y. Chung, B. J. McCoy, J. M. Smith and D. E. Cagliostro, *AIChE J.*, **39**, 1834 (1993).
11. G. Y. Chung, B. J. McCoy, J. M. Smith and D. E. Cagliostro, *Chem. Eng. Sci.*, **47**, 311 (1992).
12. G. Y. Chung and B. J. McCoy, *J. Am. Ceram. Soc.*, **74**, 746 (1991).
13. M. S. Cho, J. W. Kim and G. Y. Chung, *Korean J. Chem. Eng.*, **13**, 515 (1996).
14. T. Tago, M. Kawase, Y. Ikuta and K. Hashimoto, *Chem. Eng. Sci.*, **56**, 2161 (2001).
15. K. H. Bang, G. Y. Chung and H. H. Koo, *Korean J. Chem. Eng.*, **28**, 272 (2011).
16. D. G. Hwang and G. Y. Chung, *Korean J. Chem. Eng.*, **29**, 1266 (2012).
17. K. Jiang, H. Li and M. Wang, *Mater. Lett.*, **54**, 419 (2002).
18. H. J. Li, K. Y. Jiang and K. Z. Li, *Mater. Lett.*, **57**, 2366 (2003).
19. J. H. Kim, H. M. Lee, D. W. Kang, K. M. Lee and C. K. Kim, *Korean J. Chem. Eng.*, **33**, 2711 (2016).
20. J. Ren, K. Li, S. Zhang, X. Yao and H. Li, *Ceram. Int.*, **42**, 2887 (2016).
21. J. Ren, K. Li, S. Zhang, X. Yao and S. Tian, *Mater. Design*, **65**, 174 (2015).
22. P. Delhaes, *Carbon*, **40**, 641 (2002).
23. B. Reznik, D. Gerthsen and K. J. Huttinger, *Carbon*, **39**, 215 (2001).
24. S. Vaidyaraman, W. J. Lackey, P. K. Agrawal and T. L. Starr, *Carbon*, **34**, 1123 (1996).
25. J. Li, A. Kazakov and F. L. Dryer, *J. Phys. Chem.*, **108**, 7671 (2004).
26. P. A. Tesner, in *Chemistry and Physics of Carbon*, Vol. 19, P. A. Thrower Ed., Marcel Dekker, New York (1984).